Model Predictive Control of 3-Level T-type Converter For Grid-tie Application

Shivani Soni
Department of Electrical Engineering
National Institute of Technology
Warangal, India
shivanisoni.myr25@gmail.com

Dr. D. Sreenivasarao
Department of Electrical Engineering
National Institute of Technology
Warangal, India
srinudee@nitw.ac.in

2024 IEEE International Conference on Power Electronics, Drives and Energy Systems (PEDES) | 979-8-3503-7247-2/24/$31.00 ©2024 IEEE | DOI: 10.1109/PEDES61459.2024.10960940

***Abstract*—A finite control set model predictive control of 3-Level T-type converter for grid tie application, with decoupled active and reactive power control with addition to dc link voltage balancing has been investigated and presented in this project. Also, one notable constraint associated with employing MPC is the variable switching frequency. This challenge can be mitigated by comparing the switching states with a carrier wave of constant frequency. Nevertheless, fine-tuning the weighting factors poses a formidable challenge, particularly as and when count of constraint to be included in designing of a cost-function rises. Consequently, in this proposed approach, the complexity of this tuning process is mitigated by adopting a MCDM technique, specifically VIKOR. Through simulation, the suggested predictive control algorithm is verified and demonstrates the ability to track and regulate the input unity power factor**

***Index Terms*—Model Predictive Control (MPC), Multi-Criteria Decision-Making (MCDM), VIseKriterijumska Optimizacija I Kompromisno Resenje (VIKOR)**

I. Introduction

Power electronics converters have become essential elements across a spectrum of applications, encompassing industrial operations, renewable energy utilization, electric vehicle battery charging, and the smart grid infrastructure [1]. In recent times, with the advancement control techniques of these converters have raised to prominence as one of the focal points of both academic and industrial research endeavors. These converters are typically categorized into two main types: two-level converters and multi-level converters (MLCs). While former are characterized by their simplicity, cost-effectiveness, and reduced component count, and later as it offers superior power quality and enhanced efficiency. Consequently, MLCs are progressively being adopted as replacements for traditional two-level converters [2].

TWO-LEVEL (2-L) voltage source converters (VSCs) are commonly used to link distributed energy resources (DERs) to micro grids (MGs). However, for medium and high-power applications, multilevel (M-L) VSCs are proven as great alternative to traditional 2-L VSCs, offering enhanced output waveform quality and reducing voltage stress on power semiconductor devices. Also the adoption of M-L VSCs often leads to the utilization of smaller AC filters, as the number of level increase leads to the output closer to sine wave which further leads to low THD and smaller ac filter values [3].

The traditional control strategies used for these converters, including direct power control (DPC) [4], virtual flux-oriented PWM control [5], and voltage-oriented control (VOC) [6], all depend on a PI controller to meet control goals. Active and reactive power is indirectly controlled in VOC control by adjusting input currents. The required current references for DC link voltage control are produced via the outer PI control loop. On the other hand, in DPC, measured line currents are used to calculate active and reactive power, which is then compared to reference power. Switching states are chosen from a predetermined lookup table based on power faults. The difficulty in using these traditional control methods lies in the PI controller's tuning, which can be challenging.

Compared to the classical controllers outlined above, model predictive control (MPC) has received a lot of attention for its seamless integration of constraints and non-linearities, rapid dynamic response, and simplicity and intuitiveness [6]. One further noteworthy benefit of MPC over classical controllers is its ability to operate independently of pulse width modulation specifications. Using a discrete-time system model, the MPC algorithm predicts how control variables will behave in the future over a predetermined time frame and chooses the best course of action to minimise a cost function. Several control objectives, including current tracking, real/reactive power tracking, and speed and flux monitoring in electrical drives, can be stated using this cost function in MPC. By utilising these benefits, MPC has discovered numerous uses in the power.

A finite control set model predictive control of 3-Level T-type converter with decoupled active and reactive power control with addition to dc link voltage balancing has been investigated and presented in this project.Also, one notable constraint associated with employing MPC is the variable switching frequency. This challenge can be mitigated by comparing the switching states with a carrier wave of constant frequency [13]. Nevertheless, fine-tuning the weighting factors

poses a formidable challenge, particularly as and when count of constraint to be included in designing of a cost-

978-1-5386-5541-2/18/$31.00 ©2018 IEEE

function rises. Consequently, in this proposed approach, the complexity of this tuning process is mitigated by adopting a MCDM technique, specifically VIKOR [14]. In this method facilitates initial rankings and identifies the best switching state out of the possible switching sates and applied to converter in the next instant. This suggested control technique makes use of the power converter's discrete character to forecast how the input system variables will behave in the future.

Additionally, the technique chooses the switching state for firing the converter in the subsequent sample interval that minimises Q (vikor index) [14]. The FCS-MPC approach promptly seeks and implements the optimal inverter switching state to fulfil specific objectives, such as minimizing the error or disparity between actual and reference dc-link voltage. This ensures effective control of both power components (P and Q) to align with their respective reference values along with dc link balancing and constant switching frequency.

Firstly the mathematical modelling of the converter connected to grid is shown and then the proposed algorithm is discussed. And,then in simulation and results comparison between conventional and proposed algorithm is discussed.

II. Mathematical Modelling of System

A. Rectifier Model

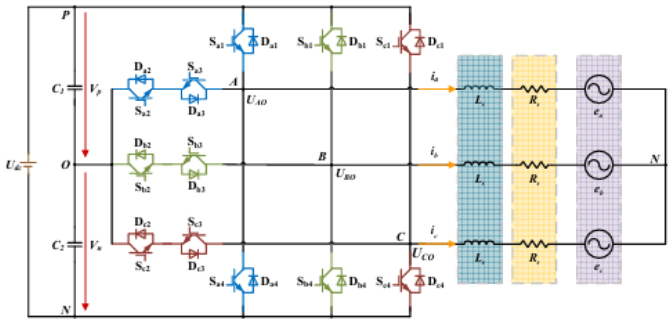

Fig. 1. Circuit Diagram of T-type Converter Connected to Grid[8]

The T-type three-phase, which is a modified NPC (Neutral Point Clamped) with a reduced switch count, has a three-level inverter topology that consists of three bridge arms, each with four power switches denoted as S_{a_x}, S_{b_x}, S_{c_x}, S_{d_x} ($x = 1$ to 4). Taking bridge arm 'a' as the point of reference, we can observe the following operational behaviour: When S_{a1}, S_{a2} are off and S_{a3}, S_{a4} are on, the bridge arm's output is $\frac{U_{dc}}{2}$ which is true for any direction of current, and this state is referred to as 'P'. Conversely, with S_{a2}, S_{a3} active and S_{a1}, S_{a4} inactive, the output is $-\frac{U_{dc}}{2}$, also independent of current direction, and is designated as 'N'. In the scenario where S_{a3}, S_{a4} are off and S_{a1}, S_{a2} are active, the output remains at zero irrespective of the current flow, and this is labelled as 'O' [8].

As,there are three phases and three distinct levels in each phase of the inverter, which means that there are a total of $2^3 = 27$ possible combinations of voltage vectors.The hexagon shown in fig.2 below displays each of the 27 voltage vectors together with the accompanying switching state [8].

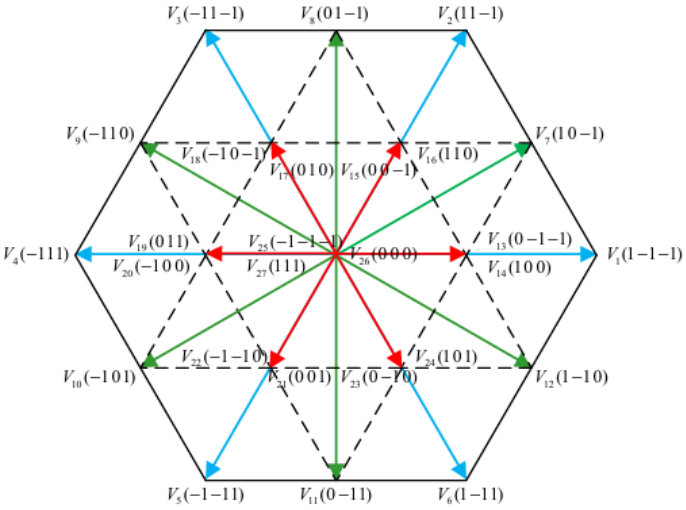

Fig. 2. Voltage Vectors and Corresponding Switching States

The voltage vector, which is determined by the inverter's switching state, can be written as follows in the coordinate system [8]:

$$U_\alpha(k) = \frac{U_{dc}(2S_a - S_b - S_c)}{6} \tag{1}$$

$$U_\beta(k) = \frac{\sqrt{3}\,U_{dc}(S_b - S_c)}{6} \tag{2}$$

Apply KVL to the circuit shown in fig.1

$$u_{an} = R_s i_a + L_s \frac{di_a}{dt} + e_a \tag{3}$$

$$u_{bn} = R_s i_b + L_s \frac{di_b}{dt} + e_b \tag{4}$$

$$u_{cn} = R_s i_c + L_s \frac{di_c}{dt} + e_c \tag{5}$$

Apply Clark transformation:

$$u_\alpha = R_s i_\alpha + L_s \frac{di_\alpha}{dt} + e_\alpha \tag{6}$$

$$u_\beta = R_s i_\beta + L_s \frac{di_\beta}{dt} + e_\beta \tag{7}$$

Euler's approximation can be used to determine the rate of change of the currents i_α and i_β in a single sample period, as indicated below:

$$\frac{di_\alpha}{dt} = \frac{i_\alpha(k+1) - i_\alpha(k)}{T_s} \tag{8}$$

$$\frac{di_\beta}{dt} = \frac{i_\beta(k+1) - i_\beta(k)}{T_s} \tag{9}$$

The following can be used to get the expected value of current $i_\alpha(k+1)$, $i_\beta(k+1)$ based on the equations:

$$i_\alpha(k+1) = i_\alpha(k) + \frac{T_s}{L_s}\left(e_\alpha(k) - u_\alpha(k) - R_s i_\alpha(k)\right) \tag{10}$$

$$i_\beta(k+1) = i_\beta(k) + \frac{T_s}{L_s}\left(e_\beta(k) - u_\beta(k) - R_s i_\beta(k)\right) \tag{11}$$

At the k^{th} sample time, the instantaneous active and reactive power are provided by:

$$P(k) = u_\alpha i_\alpha + u_\beta i_\beta \tag{12}$$
$$Q(k) = u_\beta i_\alpha - u_\beta i_\alpha \tag{13}$$

Within the $(k+1)^{\text{th}}$ sample interval, the instantaneous active and reactive power are provided by:

$$P(k+1) = u_\alpha(k+1)i_\alpha(k+1) + u_\beta(k+1)i_\beta(k+1) \tag{14}$$
$$Q(k+1) = u_\beta(k+1)i_\alpha(k+1) - u_\alpha(k+1)i_\beta(k+1) \tag{15}$$

The grid voltage components u_α and u_β can be considered constant during the sample period because to the low variation of the grid voltage in relation to the sampling and switching frequencies, that is, $u_\alpha(k+1) = u_\alpha$ and $u_\beta(k+1) = u_\beta$.

For voltage balancing, the equations involved are as follows: According to Ohm's law, the current through the resistors is given by [15]:

$$i_{\text{dc1}} = \frac{V_{C1}}{R_{\text{load}}} \tag{16}$$
$$i_{\text{dc2}} = \frac{V_{C2}}{R_{\text{load}}} \tag{17}$$

The voltage difference is given by:

$$\Delta V_{\text{dc}}(k) = V_{C1} - V_{C2} \tag{18}$$

The capacitor currents are given by [15]:

$$i_{c1} = i_{\text{dc1}} - (k_a i_a + k_b i_b + k_c i_c) \tag{19}$$
$$i_{c2} = i_{\text{dc2}} + (k_a i_a + k_b i_b + k_c i_c) \tag{20}$$

Where k_a, k_b, k_c are given by:

$$k_x = \begin{cases} 1 & \text{if } (S_x = 1) \\ 1 & \text{if } (S_x = -1) \\ 0 & \text{Otherwise} \end{cases} \tag{21}$$

Where $x = a, b, c$.

Thus, the difference between the capacitor voltages at the $k+1$ instant is given by [15]:

$$\Delta V_{\text{dc}}(k+1) = \frac{T_s}{C}(i_{C1} - i_{C2}) + \Delta V_{\text{dc}}(k) \tag{22}$$

III. Proposed Algorithm and Controller Design

The block diagram of the suggested method shown in fig. 3 is included in this section and design aspects of the controller is discussed in detail.

Starting with the cost functions of the algorithm consist of three terms. The sum of squares of the differences between the reference and anticipated values of the active and reactive powers makes up the first term in the cost function. Thus, we define the cost function as

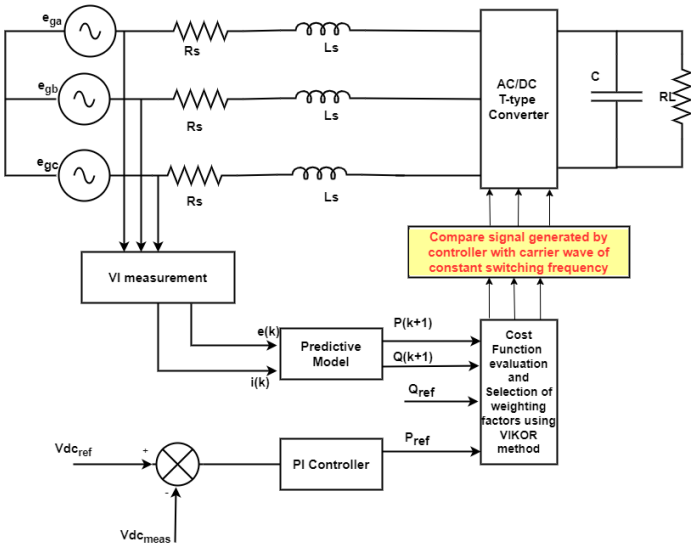

Fig. 3. Block Diagram of Proposed Algorithm

The first cost function g_1 is given by:

$$g_1 = (Q_{\text{ref}} - Q_{k+1})^2 + (P_{\text{ref}} - P_{k+1})^2 \tag{23}$$

The second cost function represents the disparity between the two DC link capacitors, V_{C1} and V_{C2}, and is given by:

$$g_2 = (\Delta V_{\text{dc}}(k+1))^2 \tag{24}$$

Now, when all of the previously defined cost functions are combined with appropriate weighting factors, such as λ_1 and λ_2, the whole cost function as calculated using the usual method is as follows:

$$g = \lambda_1 g_1 + \lambda_2 g_2 \tag{25}$$

However, adjusting the weighting factors presents a significant challenge, especially when the count of constraints within the cost function increases. As a result, the proposed approach mitigates the complexity of this tuning process by employing a MCDM technique, namely VIKOR. This approach aids in establishing initial rankings and determining the best switching state from the available options, which is then applied to the converter in the subsequent instant [14]. Implementation of VIKOR method in order to find the best switching state:

Step 1: Generation of Cost Function Matrix

As stated above, g_1 represents the cost function related to active and reactive power control, and g_2 represents the cost function related to balancing of the two capacitor voltages, i.e., DC link balancing control. Now, in this method, we first need to create the cost function matrix, which is formed by individually evaluating the cost functions for all the available switching states. As we have 27 switching states corresponding to all the 27 voltage vectors, the C_{ij} matrix formed will be of order 27×2 [14].

$$\begin{bmatrix} C_{11} & \cdots & C_{12} \\ \vdots & \ddots & \vdots \\ C_{271} & \cdots & C_{272} \end{bmatrix}_{27\times 2} \tag{26}$$

Step 2: Determine the positive and negative optimal values for each cost function after evaluating the cost functions for each switching state. In each column of C_{ij}, the positive optimal value denotes the maximum and the negative optimal value, the minimum. Since the goal of this strategy is to reduce error, the negative ideal value is thought to be the best option [14].

article amsmath

$$\begin{aligned} C_1^- &= (\min C_{i1}); \quad C_2^- = (\min C_{i2}); \\ C_1^+ &= (\max C_{i1}); \quad C_2^+ = (\max C_{i2}); \end{aligned} \tag{27}$$

Step 3: The utility measure in step three the average scores are marked by Si and the scores of the worst group are shown by the regret measure R_i [14].

$$S_i = \sum_{j=1}^{2} w_j * \frac{C_j^- - C_{ij}}{C_j^- - C_j^+} \tag{28}$$

$$R_i = \left[w_j * \frac{C_j^- - C_{ij}}{C_j^- - C_j^+} \right] \tag{29}$$

According to the VIKOR technique, In the preceding equations, W_j denotes the weight given to the j^{th} cost function. All weights added together must always equal one, i.e., [14].

$$\sum_{j=1}^{n} W_j = 1 \tag{30}$$

Step 4: Using the VIKOR index (Q), the best switching state is selected from the various options in this method's last step. The method used to calculate Q is... [14]

$$Q = m \left[\frac{S_i - S^-}{S^+ - S^-} \right] + (1-m) \left[\frac{R_i - R^-}{R^+ - R^-} \right] \tag{31}$$

Within this context, the group utility factor m is often set to 0.5. The superscripts $'-'$ and $'+'$ indicate the minimum and maximum values, respectively. Every switching state has its Q value calculated, and the state with the lowest Q value is the best one to use in the control phase that follows.

IV. Simulation Results

The effectiveness of T-type converter for grid-tie application is validated by simulating the proposed control scheme in MATLAB Simulink. The simulation parameters are listed in Table I, and the simulation was conducted with a sampling period of T = 10 µS.Here comparison of conventional MPC and proposed MPC is presented. Fig.4 represents the block diagram of conventional MPC in which optimal state of switching is directly given to the converter which leads to variable frequency which sometimes can be higher frequency which results in higher switching losses. Table 1 shows the parameters used in the simulation

Parameter	Value
Line Resistance R_s	0.2 Ω
Line Inductance L	10 mH
DC-Link Capacitance C_1, C_2	4700 μF, 4700 μF
Grid Frequency F	50 Hz
DC-Link Reference $V_{dc(ref)}$	800 V
Sampling Period T_s	10 μs
Weighing Factors W_1, W_2	0.99, 0.01
Load Resistance R_L	100 Ω
PI Controller Gains K_p, K_i	1, 100
Phase Voltage Peak e_g	338.8 V

TABLE I
System Parameters

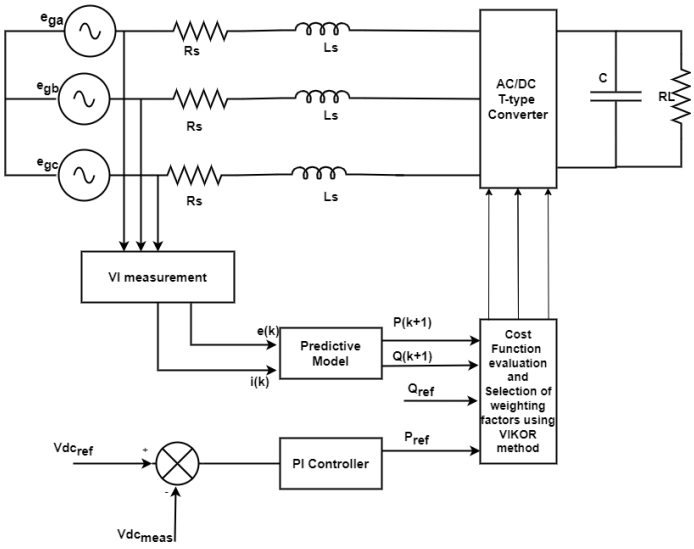

Fig. 4. Block Diagram of Conventional MPC

It can be observed from Fig. 5 that the reference DC-link voltage is initially 700V, and it changes to 800V at $t = 5$ s. The controller successfully tracks the updated reference voltage, demonstrating a strong dynamic response to the voltage change. Fig. 6 illustrates the voltages of the two capacitors, C1 and C2, as well as the capacitor voltage balancing. Figure 7 displays the grid voltage and current waveforms for the same phase (phase-a) in this instance. One can observe that the grid currents exhibit a sinusoidal pattern and align with the grid voltage, resulting in a power factor of unity.

The THD examination of the phase-A grid current, depicted in Fig.8, indicates a resulting current THD of (4.05%) for phase A, with comparable outcomes across the other phases. These findings demonstrate compliance with international standards, as the observed THD remains below the defined maximum threshold of 5% for low voltage applications.

Variable switching frequencies caused by conventional MPC can occasionally also be extremely high, which raises switch-

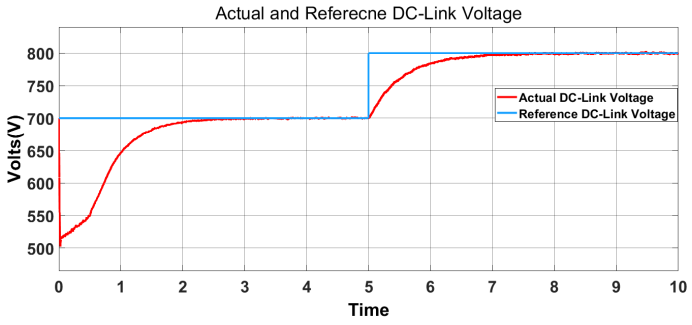

Fig. 5. Reference Voltage and Dc-Link VOltage wavefroms

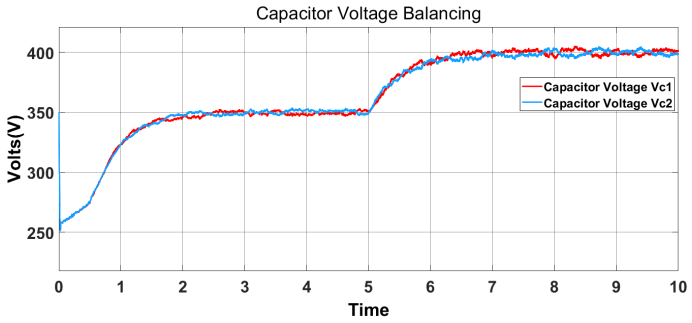

Fig. 6. Capacitor Voltages Vc1 and Vc2 Wavefroms

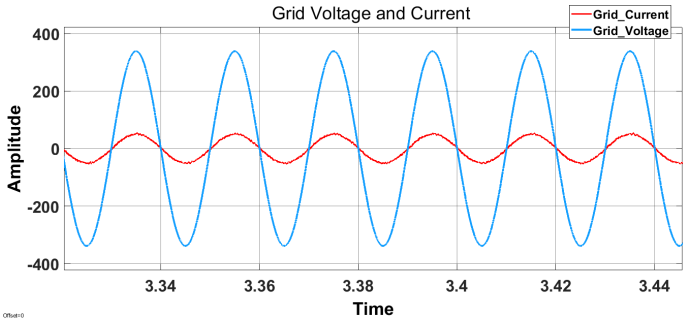

Fig. 7. Grid Voltage and Currents in-phase

ing losses even further. So, it is required to make the switching frequency constant.To overcomes this disadvantage the suggested controller is designed such that the controller chooses state which minimises the Q (vikor index) after evaluating the value of the cost function for each states. The proper switching sequence is chosen based on the minimum Q, and it is then compared with a carrier signal of constant frequency to produce switching pulses for the inverter. Fig.3 shows block diagram of proposed algorithm.Reference dc-link voltage is set as 700V and at $t = 5\,\mathrm{s}$ it is changed to 800V, and from the below fig.9, it can be analyzed that the controller is able to track the reference dc-link voltage effectively.Also it is able to track the change in reference voltages when a step change is given at t=5.Fig.10 shows capacitor voltage balancing of C1 and C2.Fig.11 shows the grid voltage and currents in-phase leading to UPF.The THD examination of the

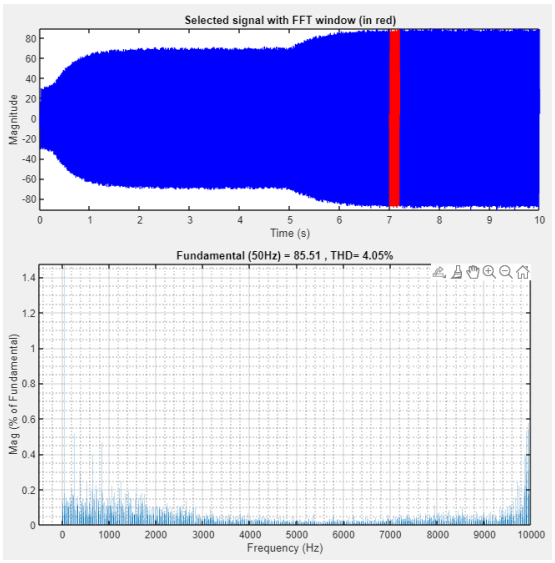

Fig. 8. THD Analysis of Grid Current

phase-A grid current, depicted in Fig.12, indicates a resulting current THD of 3.47% for phase A, with comparable outcomes across the other phases.These findings demonstrate compliance with international standards, as the observed THD remains below the defined maximum threshold of 5% for low voltage applications.Here from the THD analysis it is evident that the Proposed MPC algorithm reduces the switching frequency and also makes it constant.

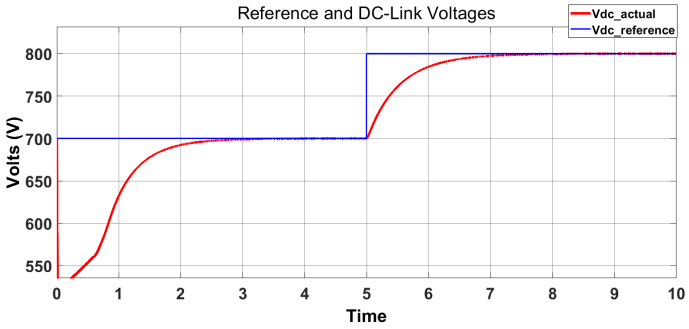

Fig. 9. Reference Voltage and DC-link voltages wave-forms

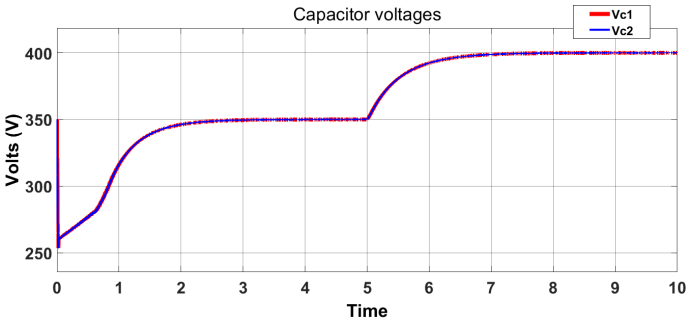

Fig. 10. Capacitor Voltages Vc1 and Vc2

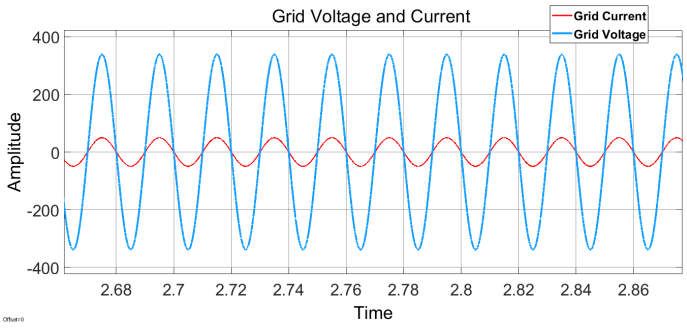

Fig. 11. Grid Voltage and Current in-phase

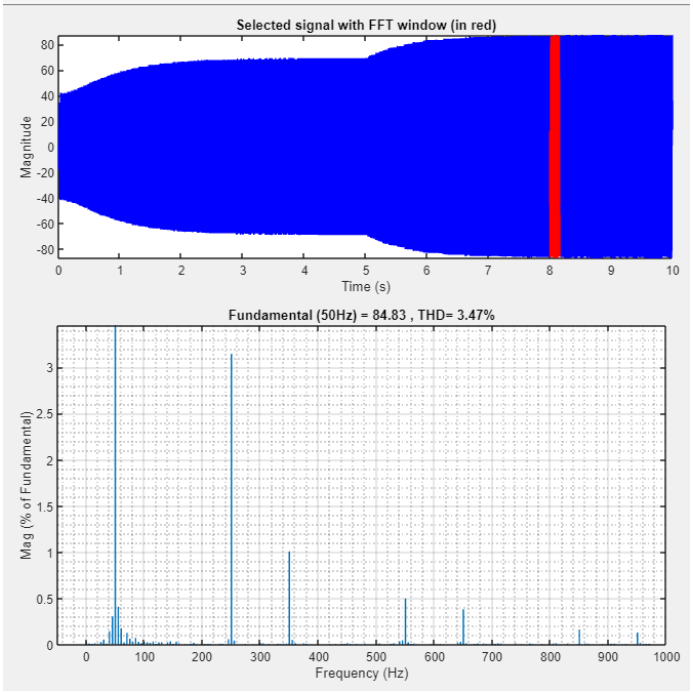

Fig. 12. THD of Grid Current

V. Conclusion

Model Predictive Control of T-type rectifier for low voltage applications is designed and verified through MATLAB/SIMULINK. In this project there are various system parameters that are being controlled such as dc-link voltage, capacitor balancing or neutral point voltage balancing, active power reactive power with constant and reduced switching frequency. Source currents are found to be balanced in the simulation experiments. By contrasting the suggested MPC algorithm with the traditional approach, it was possible to determine that, in the latter scenario, the switching frequency is variable and constant, respectively. As a result, the proposed algorithm's constant switching frequency MPC helps to greatly reduce switching losses while overcoming the variable switching frequency constraint of MPC without sacrificing THD.

References

[1] S. S. Refaat, O. Ellabban, S. Bayhan, H. Abu-Rub, F. Blaabjerg, and M. M. Begovic, *Smart Grid and Enabling Technologies*. John Wiley & Sons, 2021.

[2] H. Komurcugil, S. Bayhan, R. Guzman, M. Malinowski, and H. Abu-Rub, *Advanced Control of Power Converters: Techniques and Matlab Simulink Implementation*, no. 1. Wiley-IEEE Press, 2023.

[3] J. Weidong, L. Wang, J. Wang, X. Zhang, and P. Wang, "A carrier-based virtual space vector modulation with active neutral-point voltage control for a neutral-point-clamped three-level inverter," *IEEE Trans. Ind. Electron.*, vol. 65, no. 11, pp. 8687–8696, Nov. 2018.

[4] J. Lyu, J. Wang, W. Hu, and Y. Yan, "A neutral-point voltage controller with hybrid parameters for NPC three-level Grid connected inverters under unbalanced Grid conditions," *IEEE J. Emerg. Sel. Topics Power Electron.*, early access, Jul. 23, 2019, doi: 10.1109/JESTPE.2019.2930570.

[5] M. Schweizer, T. Friedli, and J. W. Kolar, "Comparative evaluation of advanced three-phase three-level inverter/converter topologies against two-level systems," *IEEE Trans. Ind. Electron.*, vol. 60, no. 12, pp. 5515–5527, Dec. 2013.

[6] M. Schweizer and J. W. Kolar, "Design and implementation of a highly efficient three-level T-Type converter for low-voltage applications," *IEEE Trans. Power Electron.*, vol. 28, no. 2, pp. 899–907, Feb. 2013.

[7] J. Dannehl, C. Wessels, and F. W. Fuchs, "Limitations of voltage-oriented PI current control of grid-connected PWM rectifiers with LCL filters," *IEEE Trans. Ind. Electron.*, vol. 56, no. 2, pp. 380–388, Feb. 2009.

[8] Dang C, Tong X, Yin J, Huang J, Xu Y. The neutral point-potential and current model predictive control method for Vienna rectifier. Journal of the Franklin Institute. 2017 Nov 1;354(17):7605-23.

[9] D. Zhi, L. Xu, and B. W. Williams, "Improved direct power control of grid-connected DC/AC converters," *IEEE Trans. Power Electron.*, vol. 24, no. 5, pp. 1280–1292, May 2009.

[10] P. C. Jose Rodriguez, *Predictive Control of Power Converters and Electrical Drives*. Wiley-IEEE Press, 2012.

[11] J. Rodriguez, M. P. Kazmierkowski, J. R. Espinoza, P. Zanchetta, H. Abu-Rub, H. A. Young, and C. A. Rojas, "State of the art of finite control set model predictive control in power electronics," *IEEE Trans. Ind. Informatics*, vol. 9, no. 2, pp. 1003–1016, May 2013.

[12] Chaoliang Dang, Xiangqian Tong, Jun Yin, Jingjing Huang, Yao Xu,The neutral point-potential and current model predictive control method for Vienna rectifier,Journal of the Franklin Institute,Volume 354, Issue 17,2017,

[13] A. P. Kumar, G. Siva Kumar, and D. Sreenivasarao, "Model predictive control with constant switching frequency for four-leg DSTATCOM using three-dimensional space vector modulation," *IET Gener. Transm. Distrib.*, vol. 14, pp. 3571-3581, 2020, doi: 10.1049/iet-gtd.2019.1775.

[14] A. P. Kumar, G. S. Kumar, D. Sreenivasarao, and H. Myneni, "Model predictive current control of DSTATCOM with simplified weighting factor selection using VIKOR method for power quality improvement," *IET Gener. Transm. Distrib.*, vol. 13, pp. 3649-3660, 2019, doi: 10.1049/iet-gtd.2018.6782.

[15] S. Kouro, P. Cortes, R. Vargas, U. Ammann, and J. Rodriguez, "Model predictive control—A simple and powerful method to control power converters," *IEEE Trans. Ind. Electron.*, vol. 56, no. 6, pp. 1826-1838, June 2009, doi: 10.1109/TIE.2008.2008349.